Journal of Molecular Liquids 212 (2015) 487–502

Contents lists available at ScienceDirect

Journal of Molecular Liquids

journal homepage: www.elsevier.com/locate/molliq

Supramolecular structure, molecular docking and thermal properties of azo dye complexes

A.Z. El-Sonbati [a,*], G.G. Mohamed [b], A.A. El-Bindary [a], W.M.I. Hassan [b], M.A. Diab [a], Sh.M. Morgan [c], A.K. Elkholy [a,1]

[a] Chemistry Department, Faculty of Science, Damietta University, Damietta, Egypt
[b] Chemistry Department, Faculty of Science, Cairo University, Giza, Egypt
[c] Environmental Monitoring Laboratory, Ministry of Health, Port Said, Egypt

ARTICLE INFO

Article history:
Received 25 June 2015
Received in revised form 22 September 2015
Accepted 24 September 2015
Available online xxxx

Keywords:
Azo rhodanine derivatives
Molecular docking
Pt(II)/Rh(III) and Ir(III) complexes
TGA
Quantum chemical parameters

ABSTRACT

The complexes of $[Pt(L_n)_2]$ and $[M(L_n)_2(OH_2)_2]Cl$ (M = Rh(III) and Ir(III)), where L_n = monobasic bidentate 5-(4-derivatives phenylazo)-2-thioxo-4-thiazolidinone (HL_n) have been prepared and characterized by elemental analyses, conductivity measurements, magnetic susceptibility measurements and spectroscopic (IR, Uv.-Vis. and ^1H NMR) studies. The X-ray diffraction (XRD) pattern of the ligand (HL_2) is polycrystalline nature. The molecular, electronic structures and quantum chemical parameters of the ligands (HL_n) were studied. Molecular docking was used to predict the binding between ligands (HL_n) and the receptor of breast cancer 3HB5 oxidoreductase. The Rh(III) and Ir(III) complexes are six-coordinate distorted octahedral, whereas Pt(II) is four coordinated. The ligand coordinates through the azo dye nitrogen atom and enolic oxygen atom after deprotonation. The molar conductivities show that all the complexes of Pt(II) are non-electrolytes while Rh(III) and Ir(III) complexes are electrolytic nature. The ligands field parameters were calculated using various energy level diagrams.

1. Introduction

Interest in coordination chemistry is increasing continuously with the preparation of organic ligands containing a variety of donor groups. Ligands with potential sulfur, oxygen and nitrogen donors, such as rhodanine and its derivatives are quite interesting which have gained special attention in the last decade, not only because of the structural chemistry and their importance in medical chemistry, but also because these materials are used as drugs and they are reported to possess a wide variety of biological activities against bacteria and fungi [1]. They are also becoming a useful model for bioinorganic processes, which has many biochemical and pharmacological applications. Great efforts have therefore been made to synthesize metal(II)/(III) complexes of high biological activity and low toxicity which are readily absorbed. Azo dyes of rhodanine derivatives are a good series of ligands capable of binding metal ions leading to metal complexes [2]. The high stable potential of rhodanine derivative complexes in different oxidation states increased the application of these compounds in a wide range. Efforts have been made to carry out detailed studies to synthesize and elucidate the structural and electronic properties of novel families of complexes with rhodanine derivatives as a novel chelating bidentate azo dyes models [1,3]. The use of protein-ligand docking has become a standard method in many studies. Molecular docking is widely used to predict protein-ligand [4] and to screen large libraries for molecules that will modulate the activity of a biological receptor.

Considerable research aimed at explaining the chemistry and biochemistry of platinum group metal complexes, which behave as cytotoxic agents, has given an impetus to the search for new antitumour agents of platinum and other transition metals. The interaction of platinum metals with biologically important molecules began when Rosenberg et al. [5], discovered that *cis*-diammine dichloroplatinum(II) (*cis*-platin) exhibited anti-cancer activity.

Azo rhodanines and their derivatives have been extensively used as ligands in transition metal coordination chemistry [6–8]. Ease of synthesis, favorable steric arrangement and variability of donor sites that these ligands possess with suitable constituents, make this family an excellent candidate for constructing new families of complexes which are of great intriguing interest for the coordination chemist. This research includes the molecular docking of synthesized compounds with the receptor of breast cancer 3HB5 oxidoreductase. The molecular and electronic structures of the ligands (HL_n) were studied as well as the calculated quantum chemical parameters. Also, the present paper describes the preparation and characterization of platinum(II), rhodium(III) and

* Corresponding author.
E-mail address: elsonbatisch@yahoo.com (A.Z. El-Sonbati).
[1] Abstracted from her Ph.D.

http://dx.doi.org/10.1016/j.molliq.2015.09.038
0167-7322/

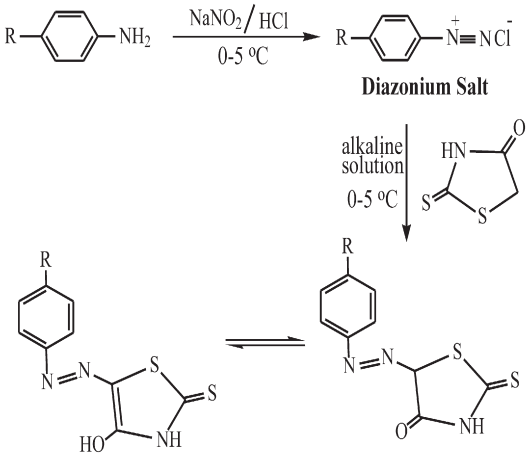

Fig. 1. R = -OCH_3 (**HL_1**), -CH_3 (**HL_2**), -H (**HL_3**), -Cl (**HL_4**) and -NO_2 (**HL_5**)**Fig. 1** The formation mechanism of azo rhodanine derivatives (**HL_n**).

Table 1
Physical properties and elemental analyses data of ligands (**HL_n**).

Compound[a]	Empirical formula	Yield %	M.p. °C	Calc. (Exp.)%		
				C	H	N
HL_1	$C_{10}H_9N_3O_2S_2$	37.45	221	44.93	3.39	15.72
	Red			(44.82)	(3.25)	(15.85)
HL_2	$C_{10}H_9N_3OS_2$	47.81	231	47.79	3.61	16.72
	Dark orange			(47.88)	(3.76)	(16.61)
HL_3	$C_9H_7N_3OS_2$	42.19	237	45.55	2.97	17.71
	Pale yellow			(45.68)	(2.80)	(17.85)
HL_4	$C_9H_6N_3OS_2Cl$	51.37	248	39.78	2.23	15.46
	Light orange			(39.65)	(2.35)	(15.58)
HL_5	$C_9H_6N_4O_3S_2$	66.087	245	38.29	2.14	19.85
	Dark yellow			(38.42)	(2.25)	(19.98)

[a] The analytical data agree satisfactory with the expected formulae represented as given in structures HL_1–HL_5. Air-stable, colored, insoluble in water, but soluble in hot ethanol, and soluble in coordinating solvent.

iridium(III) metal complexes with 5-(4-derivatives phenylazo)-2-thioxo-4-thiazolidinone (HL_n) using different spectroscopic techniques. The thermodynamic parameters of the ligands are calculated using Coats–Redfern and Horowitz–Metzger methods.

2. Experimental

2.1. Synthesis of 5-(4-derivatives phenylazo)-2-thioxothiazolidin-4-one (HL_n)

Azo rhodanine derivatives prepared by, 25 cm^3 of distilled water containing 0.01 mol conc. Hydrochloric acid was added to aniline (0.01 mol) or *p*-derivatives. To the resulting mixture stirred and cooled to 0 °C, a solution of 0.01 mol sodium nitrite in 20 cm^3 of water was added dropwise. The formed diazonium chloride was consecutively coupled with an alkaline solution of 0.01 mol 2-thioxo-4-thiazolidinone, in 10 cm^3 of pyridine as shown in Fig. 1. The colored precipitate formed was filtered through sintered glass crucible and washed several times by distilled water. The crude products were purified by recrystallization from hot ethanol and dried in a vacuum desiccator over anhydrous $CaCl_2$. The elemental analyses of ligands (HL_n) are given in Table 1. The resulting formed ligands are:

HL_1: 5-(4-methoxyphenylazo)-2-thioxo-4-thiazolidinone;
HL_2: 5-(4-methylphenylazo)-2-thioxo-4-thiazolidinone;
HL_3: 5-(phenylazo)-2-thioxo-4-thiazolidinone;
HL_4: 5-(4-chlorophenylazo)-2-thioxo-4-thiazolidinone; and
HL_5: 5-(4-nitrophenylazo) -2-thioxo-4-thiazolidinone.

2.2. Preparation of the complexes

An aqueous solution (20 cm^3) of the metal chloride of platinum(II), rhodium(III) or iridium(III) (0.01 mol) was mixed with an EtOH solution (20 cm^3) of the respective ligands (0.02 mol) in the presence of few drops of conc. HCl. The mixture was stirred for 2–16 h at room temperature to yield the desired solid chelates. For the iridium(III) complexes, the solution was boiled under reflux for 6–8 h on a water bath to effect precipitation of the solid chelates. The complexes were filter off, washed several times with EtOH followed by diethyl ether and dried in a desiccator over anhydrous $CaCl_2$. The analytical data of complexes are given in Table 2.

2.3. Measurements

Elemental microanalyses of the separated compounds for C, H and N were performed. The analyses were repeated twice to check the

Table 2
Elemental analyses data of complexes[a].

Complexes[b,c]	Calc. (Exp.)%				Cl
	C	H	N	M	
$[Rh(L_1)_2(OH_2)_2]Cl$ (1)	33.98	2.83	11.89	14.57	5.03
	(34.14)	(2.94)	(12.33)	(14.75)	(5.34)
$[Rh(L_3)_2(OH_2)_2]Cl$ (2)	33.42	2.48	13.00	15.91	5.49
	(33.54)	(2.52)	(13.44)	(16.33)	(5.53)
$[Rh(L_5)_2(OH_2)_2]Cl$ (3)	29.33	1.90	15.21	13.97	4.82
	(29.53)	(2.22)	(15.29)	(14.22)	(4.94)
$[Ir(L_1)_2(OH_2)_2]Cl$ (4)	30.16	2.51	10.56	24.16	4.46
	(30.24)	(2.59)	(10.83)	(24.39)	(4.58)
$[Ir(L_3)_2(OH_2)_2]Cl$ (5)	29.36	2.18	11.42	26.13	4.83
	(29.45)	(2.27)	(11.53)	(26.33)	(4.96)
$[Ir(L_5)_2(OH_2)_2]Cl$ (6)	26.16	1.70	13.56	23.28	4.30
	(26.26)	(1.83)	(13.76)	(23.45)	(4.58)
$[Pt(L_1)_2]$ (7)	33.00	2.20	12.93	26.83	–
	(33.21)	(2.32)	(13.12)	(26.98)	
$[Pt(L_3)_2]$ (8)	36.79	2.04	14.31	33.23	–
	(36.77)	(2.19)	(14.42)	(33.33)	
$[Pt(L_5)_2]$ (9)	28.53	1.32	14.79	25.77	–
	(28.64)	(1.44)	(14.98)	(25.89)	

L_1–L_5 are the anions of the ligands HL_1–HL_5 as given in Fig. 2.
[a] Microanalytical data as well as metal estimations are in good agreement with the stoichiometries of the proposed complexes, air stable, non-hydroscopic, high melting temperature and colored.
[b] The excellent agreement between calculated and experimental data supports the assignment suggested in the present work.
[c] All the complexes are diamagnetic.

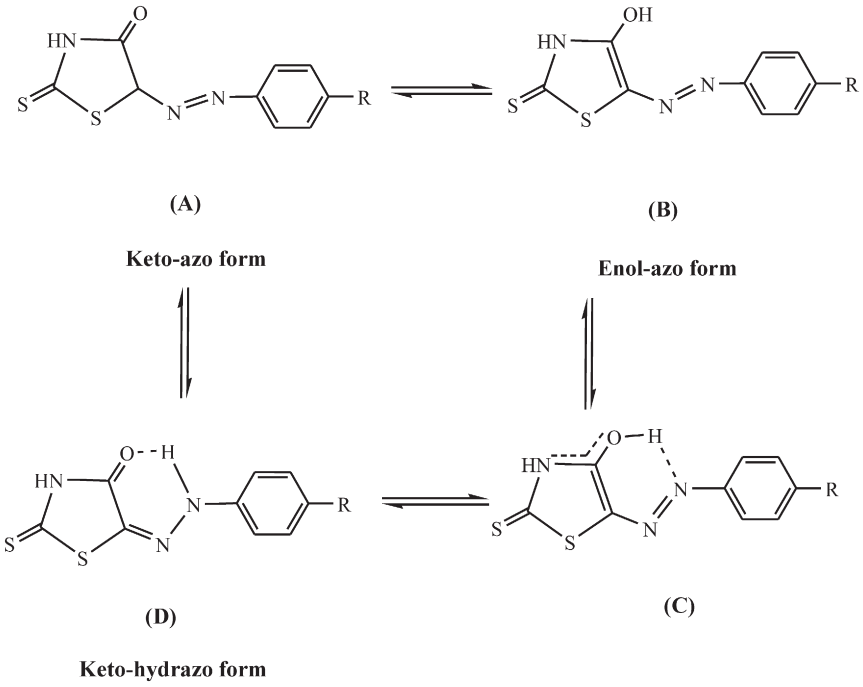

Fig. 2. The Structure of ligands (HL_n).

accuracy of the analyzed data. The ^1H NMR spectrum was obtained with a JEOL FX90 Fourier transform spectrometer with DMSO-d_6 as the solvent and TMS as an internal reference. The infrared spectra were recorded as KBr disks using a Perkin-Elmer 1340 spectrophotometer. Ultraviolet–Visible (UV–Vis) spectra of the compounds were recorded in nujol mulls using a Unicom SP 8800 spectrophotometer. X-ray diffraction analysis of the ligand (HL_2) were performed at room temperature by a Philips X-ray diffractometer equipped with utilized monochromatic Cu Kα radiation ($\lambda = 1.5418$ Å). The X-ray tube voltage and current were 40 kV and 30 mA, respectively. The magnetic moment of the prepared solid complexes was determined at room temperature using the Gouy's method. Mercury(II) (tetrathiocyanato)cobalt(II), [Hg{Co(SCN)$_4$}], was used for the calibration of the Gouy's tubes. Diamagnetic corrections were calculated from the values given by Selwood [9] and Pascal's constants. Magnetic moments were calculated using the equation, $\mu_{eff.} = 2.84\,[T\chi_M^{coor.}]^{1/2}$. Thermogravimetric analysis (TGA) measurements were investigated using Simultaneous Thermal Analyzer (STA) 6000 with scan rate 15 °C/min under dynamic nitrogen atmosphere in the temperature range from 50 to 800 °C. The molecular structures of the investigated compounds were optimized initially with the PM3 semiempirical method so as to speed up the calculations. The resulting optimized structures were fully re-optimized using ab initio Hartree–Fock (HF) [10] with 6-31G basis set. The molecules were built with the Gauss View 3.09 and optimized using Gaussian 03 W program [11]. The actual docking process in which the ligand–protein pair-wise interaction energies are calculated using a Docking Server [4]. The MMFF94 Force field was for used energy minimization of ligands molecule using a Docking Server. Gasteiger partial charges were added to the ligands atoms. Non-polar hydrogen atoms were merged and rotatable bonds were defined. Docking calculations were carried out on 3HB5 oxidoreductase protein model. Essential hydrogen atoms, Kollman united atom type charges, and solvation parameters were added with the aid of AutoDock tools [12]. Affinity (grid) maps of 20 × 20 × 20 Å grid points and 0.375 Å spacing were generated using the Autogrid program [13]. AutoDock parameter set- and distance-dependent dielectric functions were used in the calculation of the van der Waals and the electrostatic terms, respectively.

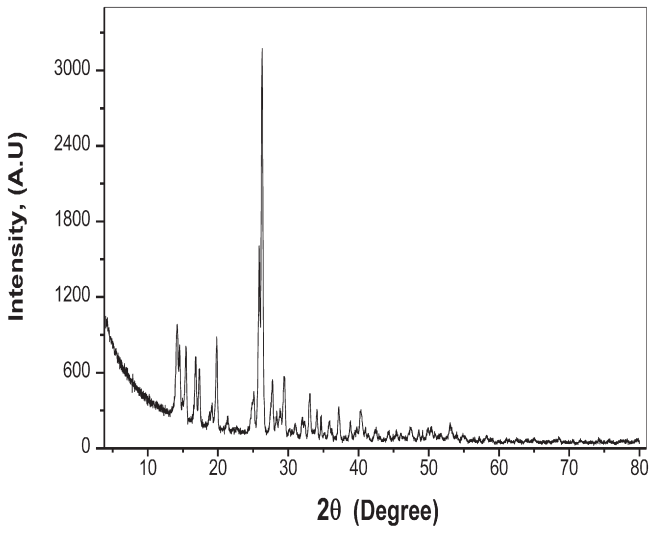

Fig. 3. X-ray diffraction pattern of ligand (HL_2).

3. Results and discussion

3.1. Characterization of the ligands

The ligands (HL_1–HL_5), gave satisfactory elemental analyses (Table 1). The molecular structures of these ligands can exist in three

Table 3
Energy values obtained in docking calculations of ligands with receptor breast cancer mutant 3HB5.

Compound	Free energy of binding (kCal/mol)	Electrostatic energy (kCal/mol)	Total intercooled energy (kCal/mol)	Interact surface
HL_1	−6.47	−0.24	−7.86	677.863
HL_2	−6.8 l	−0.16	−7.75 l	646.097
HL_3	−6.50	−0.07	−7.10	615.505
HL_4	−4.92	−0.00	−5.50	439.768
HL_5	−7.24	−0.07	−8.26	694.223

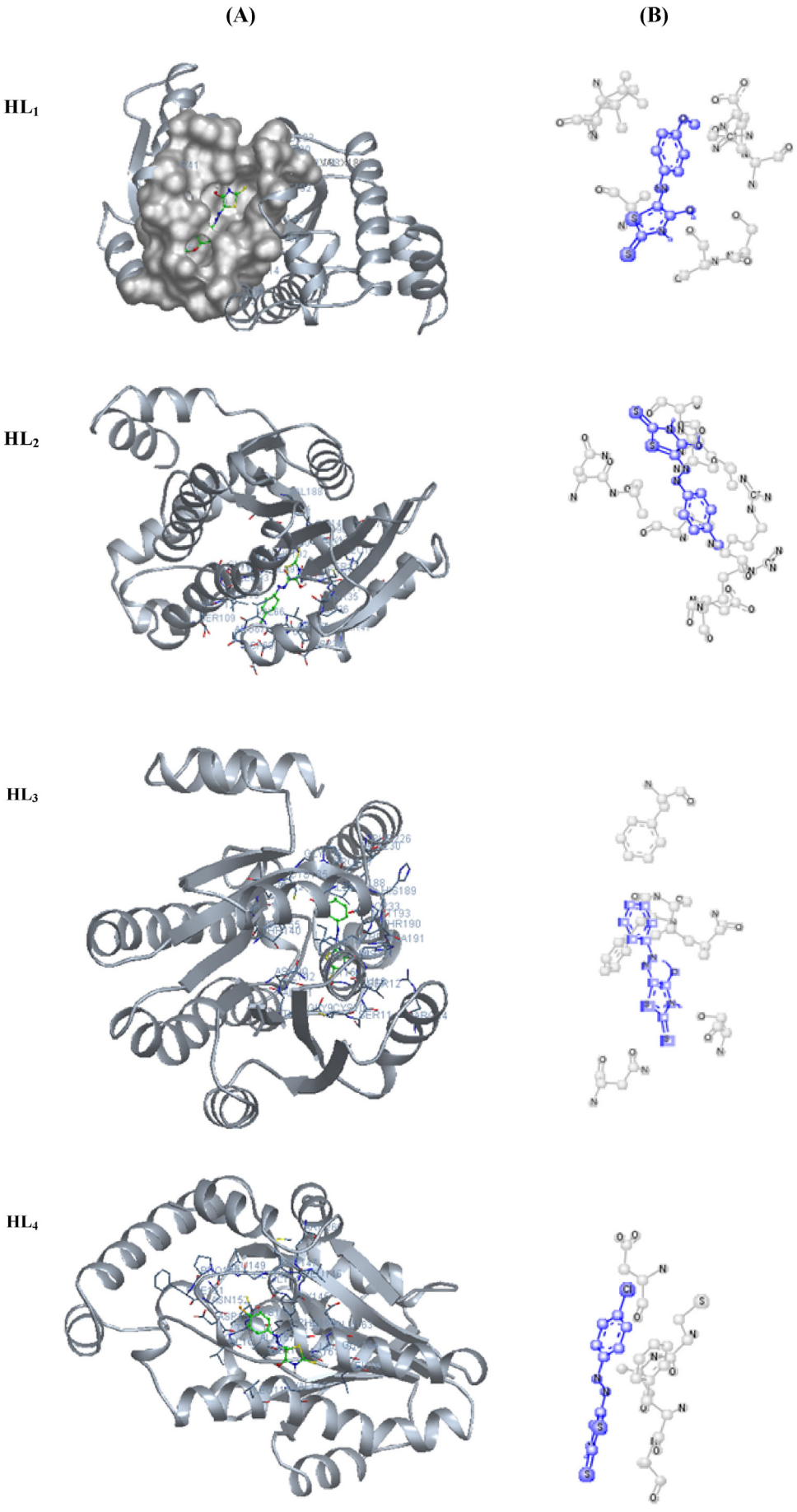
(A)
(B)
HL1
HL2
HL3
HL4

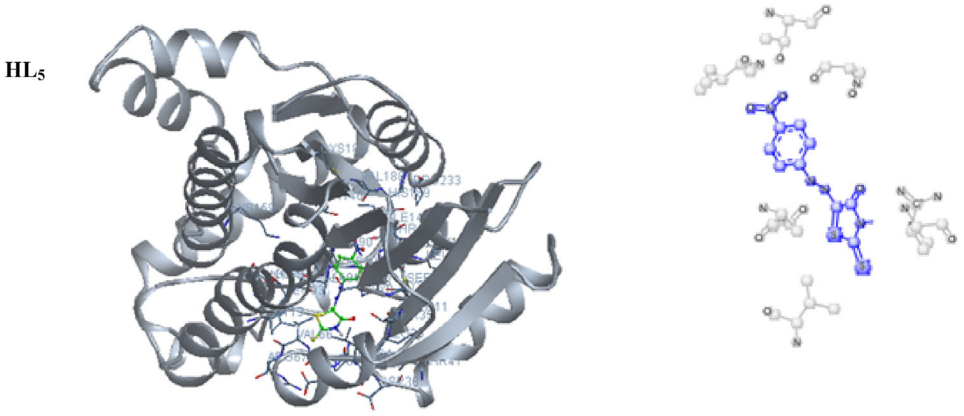

Fig. 4. The ligands (HL_n) (green in (A) and blue in (B)) in interaction with receptor breast cancer mutant 3HB5. (For interpretation of the references to color in this figure legend, the reader is referred to the web version of this article). (For interpretation of the references to color in this figure legend, the reader is referred to the web version of this article.)

tautomeric forms as shown in Fig. 2. Detailed solution and solid states studies of these ligands were carried out to establish their geometry.

The values of yield% and/or melting point is related to the nature of the *p*-substituent as they increase according to the following order *p*-(NO_2 > Cl > H > CH_3 > OCH_3) (as shown in Table 1) [14]. This can be attributed to the fact that the effective charge experienced by the d-electrons increased due to the electron withdrawing character (Cl and NO_2 groups) while it decreased by the electrons donating character of (OCH_3 and CH_3 groups). It is important to note that the existence of a methyl and/or methoxy group enhances the electron density on the coordination sites and simultaneously decreases the values of yield%.

The X-ray diffraction, XRD, pattern of the ligand (HL_2) is shown in Fig. 3. Many peaks are observed which indicate the polycrystalline nature of ligand (HL_2).

3.2. Molecular docking

Molecular docking is a key tool in computer drug design [15]. The focus of molecular docking is to simulate the molecular recognition process. Molecular docking aims to achieve an optimized conformation for both the protein and drug with relative orientation between them such that the free energy of the overall system is minimized [4].

The results of molecular docking between ligands (HL_n) and receptor breast cancer (3HB5) showed a possible arrangement between ligands and receptor (3HB5). On a docking study showing a favorable interaction between ligands and the receptor (3HB5) and the calculated of energy are listed in Table 3 and Fig. 4. 2D plot curves of docking with ligands are shown in Fig. 5. This interaction could activate apoptosis in cancer cells energy of interactions with ligands. Binding energies are most widely used mode of measuring binding affinity of ligands. Thus, decrease in binding energy due to mutation will increase the binding affinity of the ligands towards the receptor. The characteristic feature of ligands represent in presence of several active sites available for hydrogen bonding.

3.3. Geometrical structure of the ligands

Geometrical structures and electronic properties of the investigated compounds were calculated by optimizing their bond lengths, bond angles and dihedral angles. The calculated molecular structures with the optimized bond lengths of the ligands are shown in Fig. 6. The E_{HOMO} often associated with the electron donating ability of the molecule to donate electrons to appropriated acceptor molecules with low-energy, empty molecular orbital. Similarly, E_{LUMO} indicates the ability of the molecule to accept electrons. The lower value of E_{LUMO} indicates the high ability of the molecule is to accept electrons [10,17]. While, the higher is the value of E_{HOMO} of the compound, the easier is its offering electrons. The HOMO and LUMO of ligands are shown in Fig. 7.

Quantum chemical parameters of ligands are obtained from calculations such as energies of the highest occupied molecular orbital, E_{HOMO}, energies of the lowest unoccupied molecular orbital E_{LUMO}, total binding and electronic energies; heats of formation and dipole moments as presented in Table 4. Additional parameters such as separation energies, ΔE, absolute electronegativities, χ, chemical potentials, *Pi*, absolute hardness, η, absolute softness, σ, global electrophilicity, ω, [16], global softness, *S*, and additional electronic charge, ΔN_{max}, have been calculated according to the following Eqs. ((1)–(8)) [16,17]:

$$\Delta E = E_{LUMO} - E_{HOMO} \tag{1}$$

$$\chi = \frac{-(E_{HOMO} + E_{LUMO})}{2} \tag{2}$$

$$\eta = \frac{E_{LUMO} - E_{HOMO}}{2} \tag{3}$$

$$\sigma = \frac{1}{\eta} \tag{4}$$

$$Pi = -\chi \tag{5}$$

$$S = \frac{1}{2\eta} \tag{6}$$

$$\omega = \frac{Pi^2}{2\eta} \tag{7}$$

$$\Delta N_{max} = -\frac{Pi}{\eta} \tag{8}$$

The concepts of the parameters χ and *Pi* are related to each other. The inverse of the global hardness is designated as the softness [17]. From the obtained data (Table 4) we can deduced that:

Absolute hardness and softness are important properties to measure the molecular stability and reactivity. A hard molecule has a large energy gap and a soft molecule has a small energy gap. Soft molecules are more reactive than hard ones because they could easily offer electrons to an acceptor. The values of ΔN_{max} for ligands (HL_n) are calculated and found to be in the range of 0.744 - 1.022 dependent on the nature of the substituent. It was found that the values of ΔN_{max} for HL_n increase with increasing Hammett's constant coefficients (σ^R) as shown in Fig. 8.

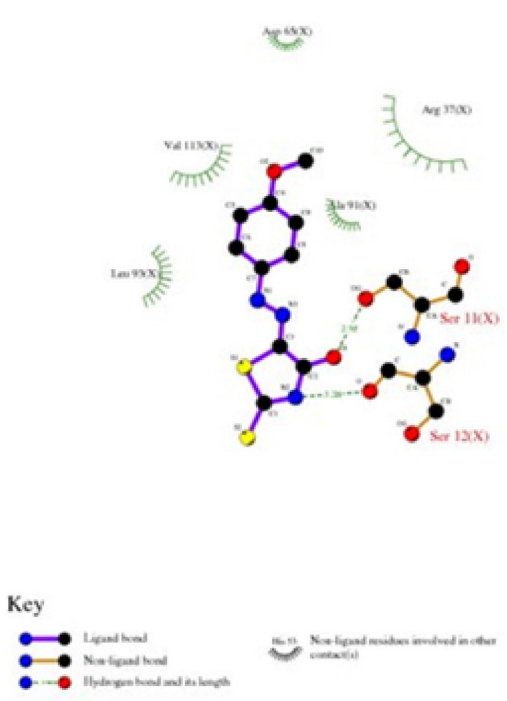

HL_1

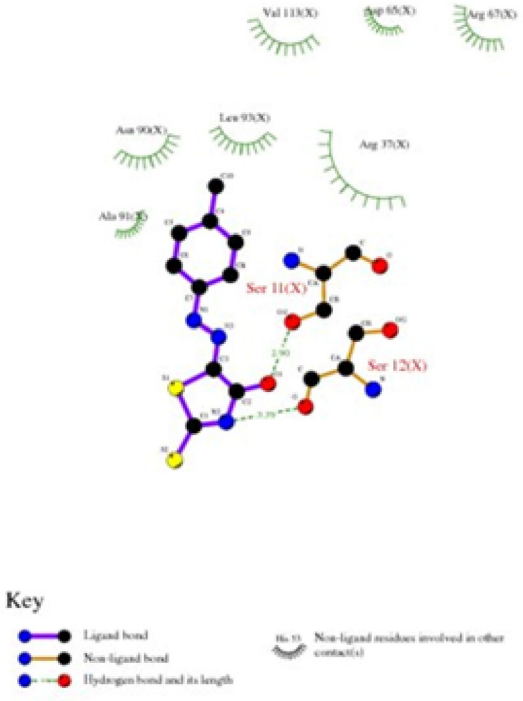

HL_2

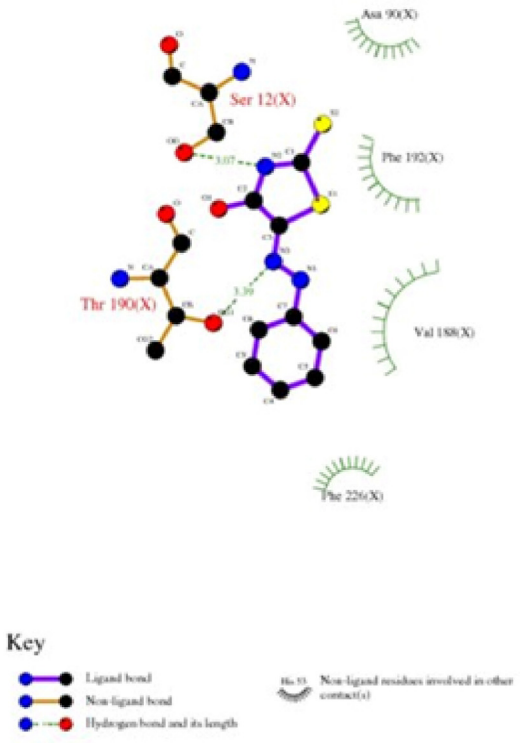

HL_3

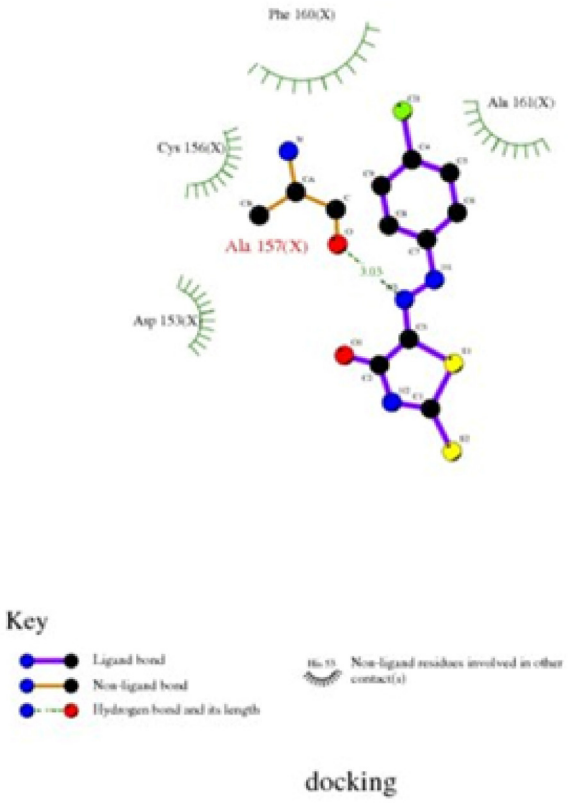

HL_4

Fig. 5. 2D plot of interaction between ligands (HL_n) with receptor breast cancer mutant 3HB5.

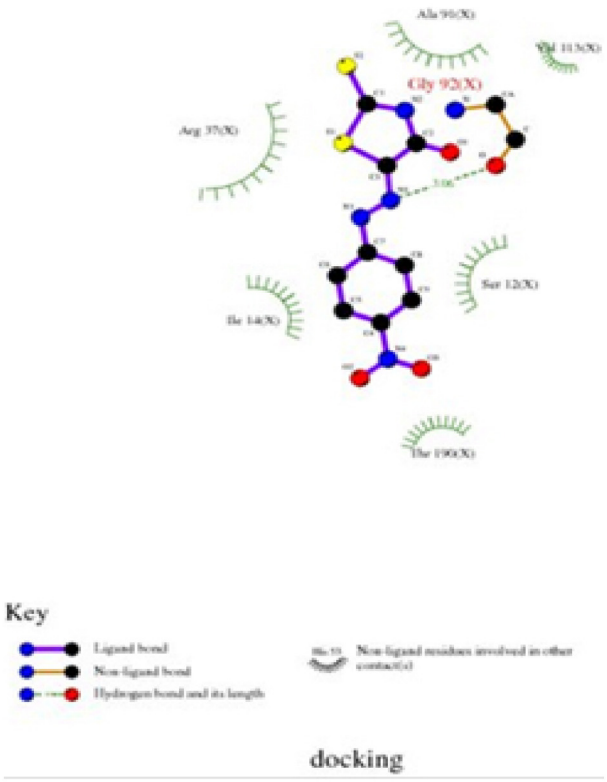

Fig. 5 (*continued*).

3.4. ^1H NMR spectra

The ^1H NMR spectra of azo rhodanine and its derivatives were investigated by El-Sonbati and coworkers [2,3,14]. The broad signals assigned to the OH protons at ~11.36–11.88 ppm are not affected by dilution. Signal for CH (~4.42 ppm), favoring formation of an intramolecular hydrogen bond with the N=N group (azo dye). The previous two protons disappear in the presence of D_2O. Absence of −CH proton signal of the ligand moiety indicated the existence of the ligand in the azo-enol form. In the meantime, the ^1H NMR of the HL_1/HL_2 exhibits signals at δ(ppm) [3.9 (s, 3H, OCH_3)]/[3.3 (s, 3H, CH_3)]. The aromatic protons have resonance at 7.10–7.45 ppm for the ligands. In the spectrum of Pt(II) complex **(7)**, the proton signal due to −OH disappears and this is a clear indication that the enolic oxygen is bonded to the metal ion after deprotonation. The position of the other proton signals has also been observed in the expected regions and has been shifted only slightly due to the coordination of the ligand to metal ion. The chemical shifts, δ, ppm owing to NH proton (of rhodanine) remain practically unchanged in the complexes, indicating that (NH of rhodanine) nitrogen does not involved in ligand coordination to the metal. Absence of CH proton signal of the rhodanine azo moiety indicated the existence of the ligand in the azo-enol form.

3.5. Spectral studies of ligands

HL_n ligands exhibits bands at 26,360-26,280 cm^{-1} (CS) (n → π*), 30,560-30,260 cm^{-1} (CO) (n → π*), 32,980-33,180 cm^{-1} (H-bonding and association), 40,250-39,900 cm^{-1} (phenyl) (Ph-Ph*), (π-π*) [14] and 29,620-29,350 cm^{-1} transition of phenyl rings overlapped by composite broad π-π* of azo structure. In the complexes, the (n → π*) transition shifts to lower energy at 28,660 cm^{-1} and the band due to the H-bonding and association is absent as expected. Furthermore, the (CS) (n-π*) transition shifts slightly to lower energy and remains almost constant. The (CO) (n → π*) transition disappears with the simultaneous appearance of new bands, being attributed to π → π* (C = C) as a sequences of enolization. The band due to π → π* transition moves to lower energy. These shifts or disappearance of the bands are indicative of coordinating of the ligands to metal.

3.6. Structural of the metal complexes

Following the successful preparation of the ligand, attention was direct towards the chemical behavior of the ligand towards M(II)/M(III) chloride. When a mixture of ligands in ethanol was reacted with M(II)/M(III) chloride in ethanol (1:2) under reflux condition, a change in color was observed and the complex compounds precipitated. The products were purified by washing with dry ethanol, and gave elemental analyses compatible with the suggested formulae given in Table 2 according to the following general equation:

$$MCl_3 + HL_n \rightarrow [M(L_n)_2(OH_2)_2]Cl + 2\ HCl \qquad (1-6)$$

$$PtCl_2 + HL_n \rightarrow [Pt(L_n)_2] + 2\ HCl \qquad (7-9)$$

where L_n = deprotonated HL_1, HL_3, HL_5 and M = Rh(III) or Ir(III).

The resulting compounds are non-hygroscopic and air-stable solids. The C, H, N and metal percentage of these complexes are presented in Table 2. The analytical data supports the above said molecular composition for these complexes.

3.7. Molar conductance of the complexes

The molar conductance of 10^{-3} M of solutions of the complexes in DMSO is calculated at 25 ± 2 °C. It is concluded from the results that Pt(II) chelates with HL_n ligand under investigation were found to have molar conductance values in the range from 11.85 to 17.55 Ω^{-1} mol^{-1} cm^2, indicating non-electrolytic nature of these compounds and there is no counter ion present outside the coordination sphere of Pt(II) complexes [18]. This is in accordance with the fact that conductivity values for a non-electrolyte are below 50 Ω^{-1} mol^{-1} cm^2 in DMSO solution [19]. While Rh(III)/Ir(III) complexes were found to be 1:2 electrolytes [20]. Such a non-zero molar conductance value for each of the complex in the present study is most probably due to the strong donor capacity of DMSO, which may lead to the displacement of anionic ligand and change of electrolyte type [18].

3.8. IR spectra and the mode of bonding in the complexes

The bonding of the metal ion to the ligand can be clarified by comparing the IR-spectra of the complexes with those of the ligands. The IR spectra of the complexes (**1-9**) show the ligands behaves as a bidentate ligand depending on the metal salt used, the reaction conditions and the pH of the medium.

The ligands gives two bands at ~3200 and 3040 cm^{-1} due to asymmetric and symmetric stretching vibrations of N–H group and intramolecular hydrogen bonding NH…O systems (Fig. 2-D), respectively. The broad absorption band located at ~3400 cm^{-1} is assigned to νOH. The low frequency bands indicate that the hydroxy hydrogen atom is involved in keto ⇔ enol (A⇔B) tautomerism through hydrogen bonding (Fig. 2-C). The OH group (Fig. 2-B) exhibits more than one absorption band. The two bands located at 1330 and 1370 cm^{-1} are assigned to in-plane deformation and that at 1130 cm^{-1} is due νC-OH. When the OH group (Fig. 2-C) is involved in intramolecular hydrogen bond, the O…N and N…O bond distances are the same [14]. But, if such mechanism is happened in case of intermolecular hydrogen bond, the O…O and O…N bond distances are differ. However, the 860 cm^{-1} band is probably due to the out-of-plane deformation of

the –OH group. On the other hand, the two bands located at 650 and 670 cm^{-1} are identified as δ C═O and NH.

El-Sonbati et al. [2,21] made detailed studies for the different types of hydrogen bonding which are favorable to exist in the molecule under investigation:

- Intramolecular hydrogen bond between the nitrogen atom of the azo dye (—N═N—) system and hydrogen atom of the hydroxy hydrogen atom (Fig. 2-C). This is evident by the presence of a broad band centered at 3460 cm^{-1}.
- Hydrogen bonding of the OH…N type between the hydroxy hydrogen atom and the N-ph group (Fig. 2-C).

The presence of broad band located at ~3200 cm^{-1} is strong indication by νNH (Fig. 2-D). In general, the low frequency of such region from its normal position is, again due to hydrogen bond property gathered with keto ⇔ enol tautomerism.

The frequencies for the N═N stretching located in the range of 1440-1435 cm^{-1}. The region between 1500 and 900 cm^{-1} is due C–N

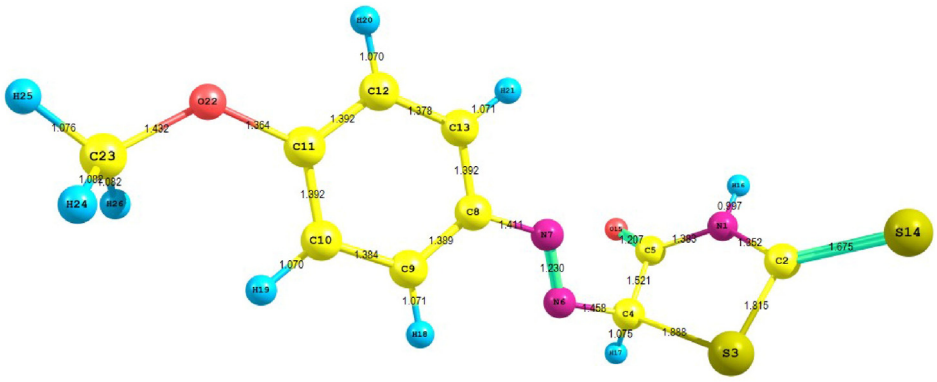

HL_1

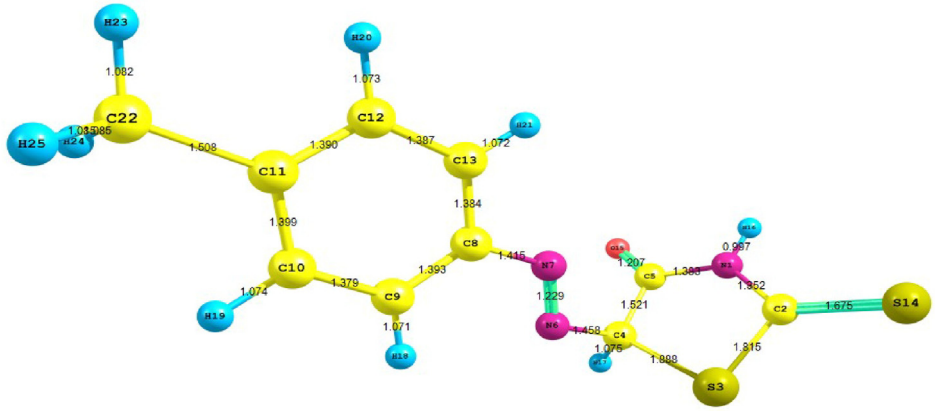

HL_2

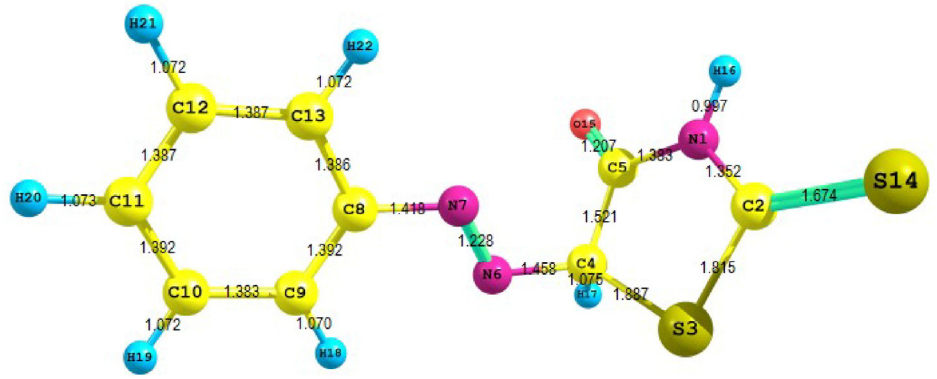

HL_3

Fig. 6. The calculated molecular structures of the ligands (HL_n).

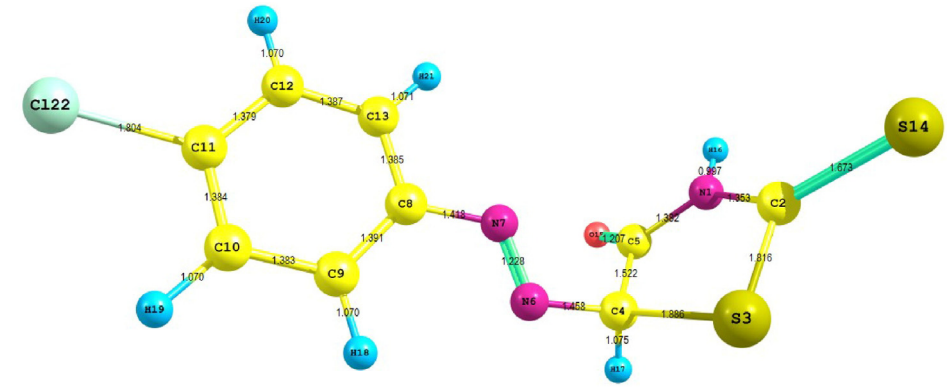

HL_4

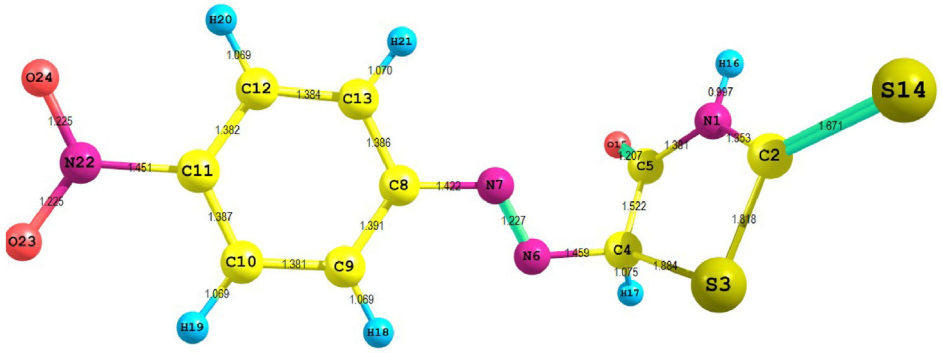

HL_5

Fig. 6 (*continued*).

stretching, N–H in plane or out of plane bending and out-of-plane C–H bending vibrations [14].

By comparing the infrared spectra of free ligands to that of the prepared complexes the following points could be outlined:

- The appearance of υ(N═N) and the disappearance of frequency bands of the υ(C═O) group in the free ligands (HL_n) suggest that there is no hydrazo-keto transformation; this is similar to that reported in the literature [2,19]. The N═N stretching frequency of azo group is shifted to lower frequency by ~ 25–35 cm^{-1} due to the involvement of one of the azo nitrogen atoms in coordination with metal ion [6–8]. This lowering of frequency can be explained by the transfer of electrons from the nitrogen atom to the metal ion due to coordination.
- In solution and in the presence of Pt(II) ions these compounds exist in a tautomerism equilibrium [1] A⇔B⇔C (Fig. 2). The internally hydrogen bonded enolic –OH band disappeared in the spectra of the metal complexes, indicating the deprotonation and formation of metal-oxygen bond. This is further supported by the shifting of υ(C–O) towards higher frequency as compared to the free ligands (HL_n) due to the conversion of hydrogen bonded structure into a covalent metal bonded structure [22].
- The appearance of new bands around ~3290 cm^{-1} and two sharp bands at ~725 and 430 cm^{-1}, the latter two can be assigned to the wagging and rocking modes of vibration of the water molecule, respectively [23] in the prepared M(III) complexes may be taken as a strong evidence for the presence of coordinated water. Such region, however, is not initially present in the free ligands. This is confirmed by the elemental analysis of these complexes (Table 2).

The ^1H NMR spectral data of the Pt(II) complexes recorded in DMSO-d_6 further substantiate the mode of coordination suggested by the IR spectral studies. In the spectrum of Pt(II) complexes, the proton signal due to –OH disappears and this is a clear induction that the enolic oxygen is bonded to the metal ion after deprotonation. Signal for methoxy proton do not show any significant change when compared to the free ligand (HL_1). Comparison of the position of the other resonance signals in the Pt(II) complexes with those of the ligand indicates downward shifting by about ~0.2 ppm in the metal complex. The positions of the other proton signals have also been observed in the expected regions and have been shifted only slightly due to the coordination of the ligand to metal ion. Thus, from the IR and NMR spectral data it is clear that the ligand is bonded to the metal ion in a bidentate fashion through the deprotonated enolate oxygen and one of the azo nitrogen atoms.

- The low intensity of bands of non-ligand appearing in the region 415–465 cm^{-1} (M–N) and 435–460 cm^{-1} (M–O).

On the basis of all these data, the molecular structure of the M(II)/M(III) complexes could be suggested based on, the absence of anion, ii) the disappearance of C═O, iii) the coordination of azo-group. It found that the ligands (L_n) is behaving as a bidentate monobasic [(O,N)] nature with respect to the evidence above, the structure for the novel complexes are tentatively proposed as shown in Fig. 9.

According to the structure shown in (Figs. 2 & 9) the HL_n ligand takes its usual anionic form (L_n) to chelate M(II)/M(III) through N- of azo group with enol group (Figs. 2-C & 9) as the potential binding sites. Attempts have been made to grow X-ray quality single crystals of these complexes; however, this has been unsuccessful so far.

3.9. Eelectronic spectra of complexes (1–9)

The electronic spectra of platinum complexes exhibit bands in the ranges of 14,710-16,050 cm^{-1} ($^1A_{1g} \rightarrow {}^1A_{2g}$), 20,100-20,980 cm^{-1} ($^1A_{1g} \rightarrow {}^1B_{1g}$) and 24,895-26,070 cm^{-1} ($^1A_{1g} \rightarrow {}^1E_g$), in order of increasing energy, respectively [24], characteristic of square planar arrangement around the metal atom. These transitions are assuming the effective symmetry to be D_{4h}. The values of ligand field parameters Δ_1, Δ_2 and Δ_3 as shown in Table 5 were calculated [25,26] using various energy level diagrams. These are consistent with the values reported earlier for such complexes [27,28]. The values of Δ_1 lie between those observed for cyanide (~30,000 cm^{-1}) and chloride complexes (~19,000 cm^{-1}) and are consistent with intermediate ligand strength [28]. The relationship between electronic spectral data (Table 5) and Hammett's substituent coefficients (σ^R) illustrated that the values of electronic spectral is related to nature of the *p*-substituent as they increase according to the following order *p*-($NO_2 < H < OCH_3$). This can be attributed to the fact that the effective charge experienced by the d-electrons decreased due to the electron withdrawing *p*-substituent (HL_5) while it increased by the electrons donating character of (HL_1). It is clear that all these values decrease with increasing σ^R. It is important to note that the existence of a methyl and/or methoxy group enhances the electron density on the coordination sites and simultaneously decreases the values of electronic spectral. The plot of single electron parameter (Δ_1) *vs.* σ [σ = Hammett's substituent coefficients (σ^R) of the substituent (R)] (Fig. 10) shows a linear relationship between Δ_1 and σ for each chromospheres. The Δ_1 and σ values are relatively insensitive to the inductive effect of the phenyl ring substituent and chiefly depend on the stereochemical factors as the redox properties. The Δ_1 values are weaker in the complex **(7)** in agreement with the more electrons donating character atom. As can be seen from (Fig. 11), the plot of υ_2/υ_1 values (for Pt complexes) versus σ [σ = Hammett's substituent coefficients (σ^R) of R] is linear. The values bare relationship insensitive to the inductive effect of the phenyl ring substituent and chiefly depend on the stereochemical factor. Furthermore, values are weaker in complex **(9)** in agreement with the more electron withdrawing *p*-substituent character.

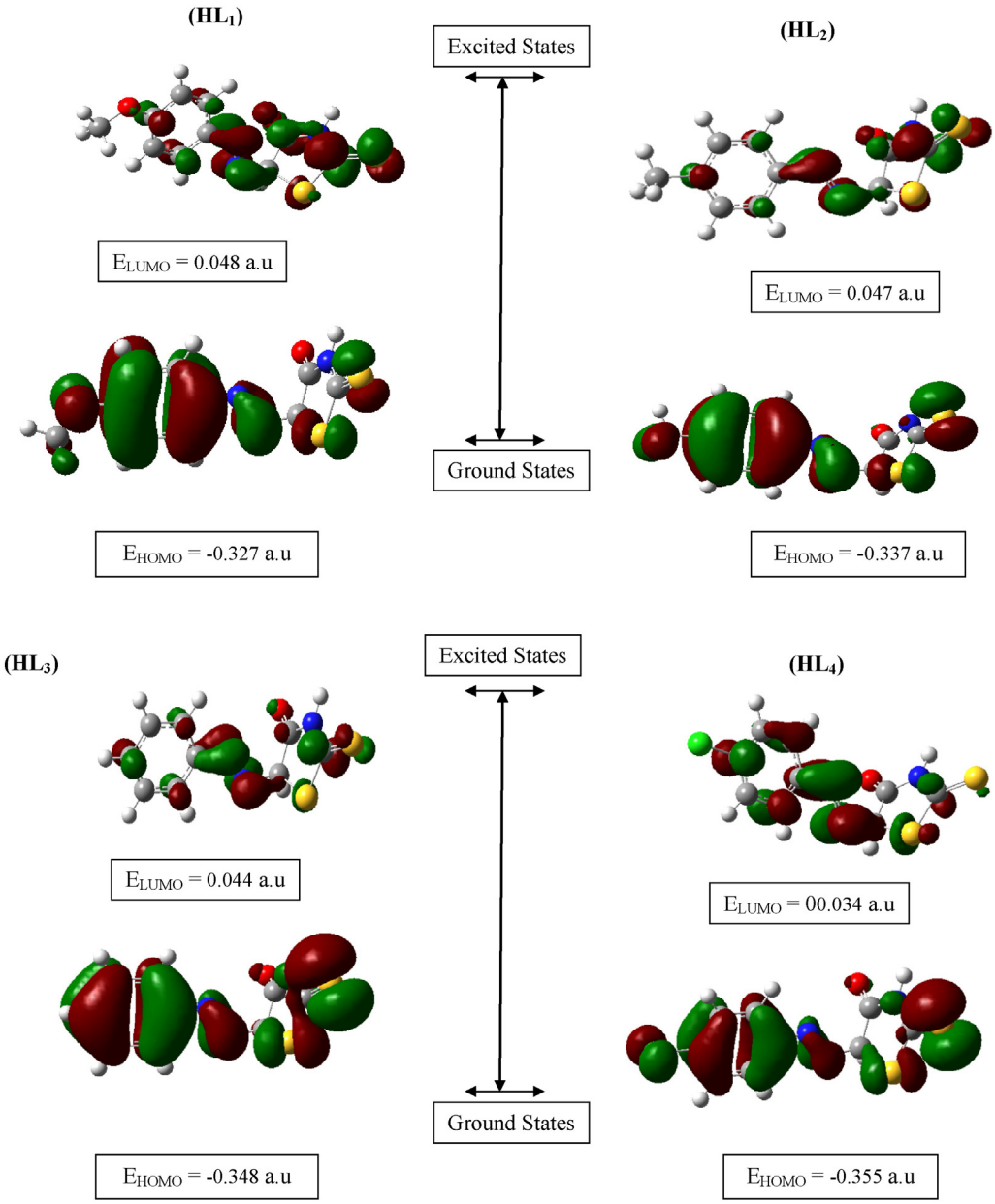

Fig. 7. The highest occupied molecular orbital (HOMO) and the lowest unoccupied molecular orbital (LUMO) of ligands (HL_n).

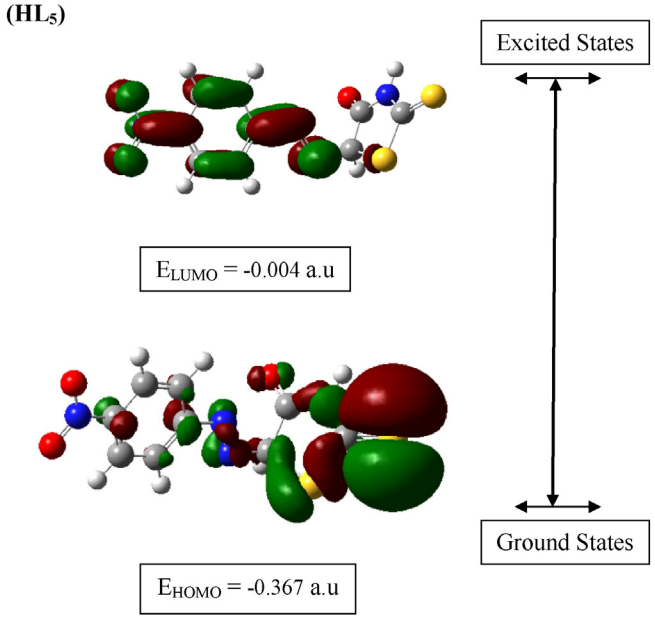

Fig. 7 (*continued*).

The electronic spectra of the radium(III) complexes (**1–3)** display bands in the ranges of 17,500–17,980 cm^{-1} ($^1A_{1g} \rightarrow {}^3T_{1g}$), 20,100–20,400 cm^{-1} ($^1A_{1g} \rightarrow {}^1T_{1g}$) and 24,700–25,100 cm^{-1} ($^1A_{1g} \rightarrow {}^1T_{2g}$) transitions in increasing order of energy which resemble those of other six-coordinate rhodium(III) complexes [29]. Electronic spectra of iridium(III) complexes (**4–6)** display bands in the ranges of 30,750–30,890 cm^{-1} ($^1A_{1g} \rightarrow {}^1T1g(\upsilon_1)$), 34,000–34,400 cm^{-1} ($^1A_{2g} \rightarrow {}^1T_{2g}$ (υ_2)) and 37,000-37,990 ($^1A_{1g} \rightarrow {}^1T_{1u}$) transitions The υ_2/υ_1 transitions have been used to evaluate the ligand field parameter (Table 5), which are comparable to data reported for other octahedral iridium(III) complexes [23] involving N and O donor atoms. The ground state in both the Rh(III) and Ir(III) complexes in an octahedral field is $^1A_{1g}$. The general pattern of the spectra indicates octahedral geometry around the metal ions [30]. The Rh(III) and Ir(III) complexes exhibit diamagnetic behavior due to their d^6 (low spin) system.

3.10. Thermal analysiss

3.10.1. Thermogravimetric analysis of ligands (HL_n)

Thermal data of ligands were characterized on the basis of thermogravimetric analysis (TGA) and differential scanning calorimetry (DSC) methods in the temperature range 50–800 °C. The TGA and DSC curves for HL_n (where n = 1, 3 and 5) is shown in Fig. 12. For HL_1 and HL_3 there are two steps of the loss of masses, while for HL_5 there are three steps. Fig. 12 reveals that the HL_1 decomposes in two steps, the first stage and weight loss starts at 200 °C with a weight loss percentage of 61.9%. The second stage, weight loss starts at 320 °C with a weight loss percentage of 38.1%. The HL_3 decomposes in two steps as shown in Fig. 12, the first stage, weight loss starts at 145 °C with a weight loss percentage of 59.8%. The second stage, weight loss starts at 400 °C with a weight loss percentage of 39.9%. The HL_5 ligand decomposes in three steps, the first stage and weight loss starts at 112 °C with a weight loss percentage of 5.4%. The second stage, weight loss starts at 225 °C with a weight loss percentage of 33.6%. The third stage, weight loss starts at 284 °C with a weight loss percentage of 58.7% [21].

The ligands (HL_3 and HL_5) show two exothermic and endothermic peaks except HL_1 ligand show one exothermic peak is shown in Fig. 12. For the HL_1 ligand the recorded DSC curve show only one exothermic peak at 220 °C. Simultaneously, the recorded DSC curve of

Table 4
The calculated quantum chemical parameters of the ligands.

Compound	E_{HOMO} (a.u)	E_{LUMO} (a.u)	ΔE (a.u)	μ (D)	T.E (a.u)	χ (a.u)	η (a.u)	σ $(a.u)^{-1}$	Pi (a.u)	S $(a.u)^{-1}$	ω (a.u)	ΔN_{max}
HL_1	−0.327	0.048	0.375	5.358	−1491.580	0.139	0.188	5.333	−0.139	2.667	0.052	0.744
HL_2	−0.337	0.047	0.384	4.554	−1416.775	0.145	0.192	5.208	−0.145	2.604	0.055	0.755
HL_3	−0.348	0.044	0.432	3.950	−1377.752	0.152	0.196	5.102	−0.152	2.551	0.059	0.776
HL_4	−0.355	0.034	0.389	2.001	−1836.627	0.161	0.195	5.141	−0.161	2.571	0.066	0.825
HL_5	−0.367	−0.004	0.363	3.712	−1581.099	0.186	0.182	5.509	−0.186	2.755	0.095	1.022

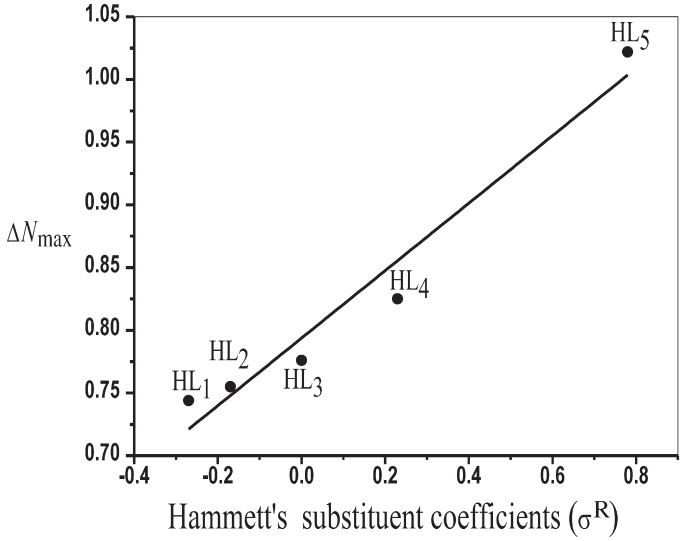

Fig. 8. The relation between Hammett's substituent coefficients (σ^R) *vs.* ΔN_{max} for ligands (HL_n).

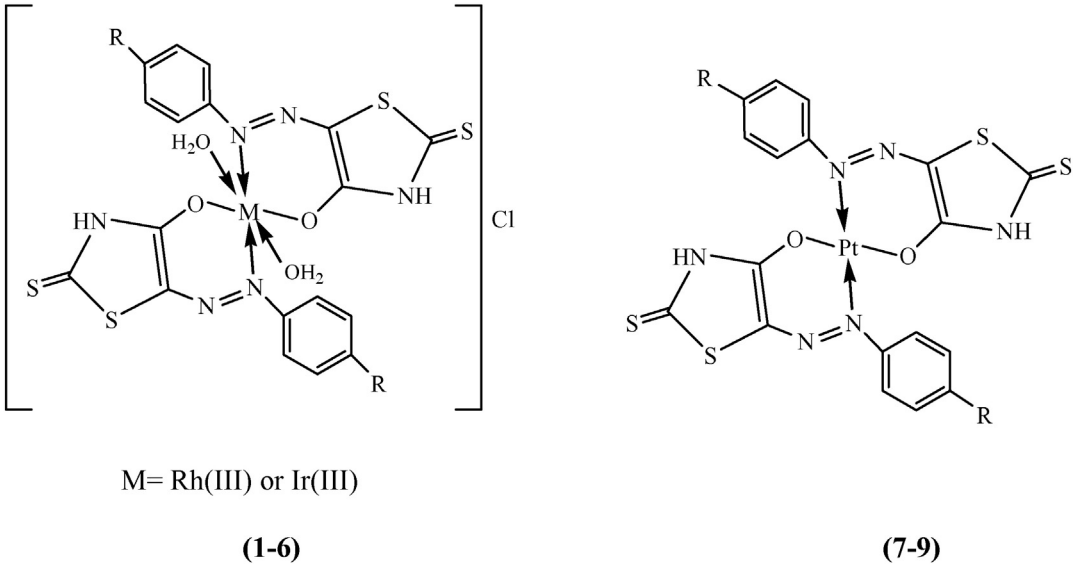

Fig. 9. The structure proposed for M(II)/(III)-complexes **(1–9)**.

the HL_3 ligand show two exothermic and endothermic peaks at 190 °C and 180 °C, respectively, while the recorded DSC curve of the HL_5 ligand show two exothermic and endothermic peaks at 245 °C and 120 °C, respectively.

3.10.2. Thermogravimetric analysis of complexes

The thermal stability and decomposition of the complexes was studies. Thermogravimetric analysis of the complexes (**1–6**) shows that the complex decomposed in four steps. These steps extended between 50 and 290 and 300–550 °C. The first and second steps accompanied with weight loss which may be attributed to the loss of $2H_2O$ and a molecule of chlorine. The next two steps, which take place within the temperature range of 350–550 °C, may involves the release of one L_n molecule. The total mass observed between 520 and 530 °C corresponded to a residue Rh_2O_3 and Ir_2O_3.

The TG curve for complexes (**7–9**), all the complexes show similar decomposition with weight losses in two stages. In the first stage, in the temperature range of ~280–320 °C is attributed to the weight loss of one molecule of ligands. The total mass loss observed at 480–540 °C was found to be stable metal oxides. The fragmentation patterns of the thermograms agree well with theoretical calculations and support the stereochemical assignments [31].

Table 5
Electronic spectra and single electron parameters.

Complex[a]	Bands cm^{-1}	Assignments	Δ_1	Δ_2	Δ_3	υ_2/υ_1
(1)	17,500	$^1A_{1g} \rightarrow {}^3T_{1g}$	–	–	–	1.157
	20,250	$^1A_{1g} \rightarrow {}^1T_{1g}$				
	24,700	$^1A_{1g} \rightarrow {}^1T_{2g}$				
(2)	17,800	-do-	–	–	–	1.129
	20,100	-do-				
	25,000	-do-				
(3)	17,980	-do-	–	–	–	1.140
	20,400	-do-				
	25,100	-do-				
(4)	30,800	$^1A_{1g} \rightarrow {}^1T_{1g}$	–	–	–	1.104
	34,000	$^1A_{1g} \rightarrow {}^1T_{2g}$				
	37,000	$^1A_{1g} \rightarrow {}^1T_{1u}$				
(5)	30,750	-do-	–	–	–	1.112
	34,200	-do-				
	37,800	-do-				
(6)	30,890	-do-	–	–	–	1.114
	34,400	-do-				
	37,990	-do-				
(7)	14,710	$^1A_{1g} \rightarrow {}^1A_{2g}$	16,810	6590	4490	1.366
	20,100	$^1A_{1g} \rightarrow {}^1B_{1g}$				
	24,895	$^1A_{1g} \rightarrow {}^1E_g$				
(8)	15,880	-do-	17,980	4956	5604	1.312
	20,836	-do-				
	25,540	-do-				
(9)	16,050	-do-	18,150	6130	4790	1.307
	20,980	-do-				
	26,070	-do-				

[a] Numbers as given in Table 2.

3.11. Calculation of activation thermodynamic parameters

The thermodynamic activation parameters of decomposition processes of complexes namely activation energy (E_a), enthalpy (ΔH^*), entropy (ΔS^*), and Gibbs free energy change of the decomposition (ΔG^*) are evaluated graphically by employing the Coast–Redfern [32] and Horowitz–Metzger [33] methods.

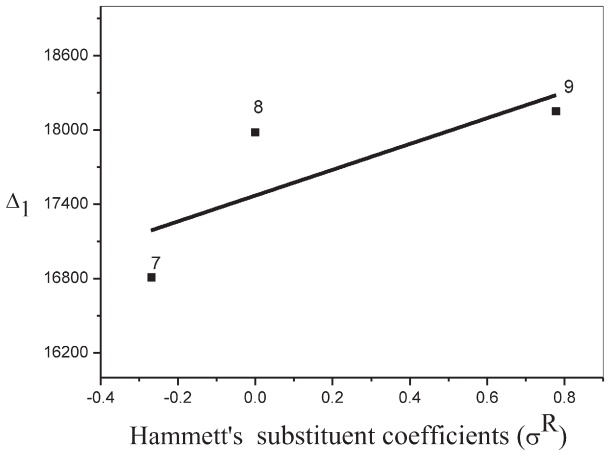

Fig. 10. The relation between Hammett's substituent coefficients (σ^R) *vs.* for Pt(II)-complexes **(7–9)**.

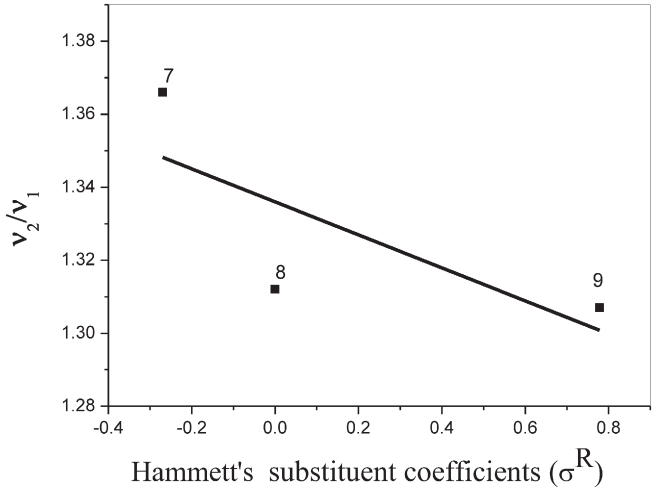

Fig. 11. The relation between υ_2/υ_1 and Hammett's substituent coefficients (σ^R) for Pt(II)-complexes **(7–9)**.

3.11.1. Coast–Redfern equation

The Coast–Redfern equation, which is a typical integral method, can represent as:

$$\int_0^a \frac{dx}{(1-\alpha)^n} = \frac{A}{\varphi}\int_{T_1}^{T_2} \exp\left(-\frac{E_a}{RT}\right)dt. \tag{9}$$

For convenience of integration, the lower limit T_1 usually taken as zero. This equation on integration gives:

$$\ln\left[-\frac{\ln(1-\alpha)}{T^2}\right] = -\frac{E_a}{RT} + \ln\left[\frac{AR}{\varphi E_a}\right]. \tag{10}$$

A plot of left-hand side (LHS) against 1/T was drawn (Fig. 13). E_a is the energy of activation in J mol^{-1} and calculated from the slop and A in (s^{-1}) from the intercept value. The entropy of activation ΔS^* in (J K^{-1} mol^{-1}) calculated by using the equation:

$$\Delta S^* = 2.303\left[\log\left(\frac{Ah}{k_B T_s}\right)\right]R \tag{11}$$

where k_B is the Boltzmann constant, h is the Plank's constant and T_s is the TG peak temperature.

3.11.2. Horowitz–Metzger equation

The Horowitz–Metzger equation is an illustrative of the approximation methods. These authors derived the relation:

$$\log\left[\frac{1-(1-\alpha)^{1-n}}{1-n}\right] = \frac{E_a\ \theta}{2.303RT_S^2}, \qquad \text{for } n\neq 1 \tag{12}$$

when n = 1, the LHS of Eq. (12) would be log[−log(1-α)] (Fig. 14). For a first order kinetic process, the Horowitz–Metzger equation may write in the form:

$$\log\left[\log\left(\frac{W_\alpha}{W_\gamma}\right)\right] = \frac{E_a\ \theta}{2.303RT_s^2} - \log\ 2.303 \tag{13}$$

where $\theta = T\text{-}T_s$, $w_\gamma = w_\alpha - w$, w_α = mass loss at the completion reaction; w = mass loss up to time t. The plot of log [log (w_α/w_γ)] *vs.* θ was drawn and found to be linear from the slope of which E_a was calculated. The pre-exponential factor, A, calculated from equation:

$$\frac{E_a}{RT_S^2} = \frac{A}{\left[\varphi\ \exp\left(-\frac{E_a}{RT_S}\right)\right]} \tag{14}$$

The entropy of activation, ΔS^*, is calculated from Eq. (11). The enthalpy activation, ΔH^*, and Gibbs free energy, ΔG^*, calculated from:

$$\Delta H^* = E_a - RT \tag{15}$$

$$\Delta G^* = \Delta H^* - T\ \Delta S^*. \tag{16}$$

The calculated values of E_a, A, ΔS^*, ΔH^* and ΔG^* for the decomposition steps for ligands are summarized in Table 6. The high values of activation energies and the entropy of activation of the ligands reflect the thermal stability of the compounds. The negative values of activation entropies (ΔS^*) indicate a more ordered activated compounds than the reactants and/or the reactions are slow [2]. The values of ΔG^* is positive considered as favorable or spontaneous reaction.

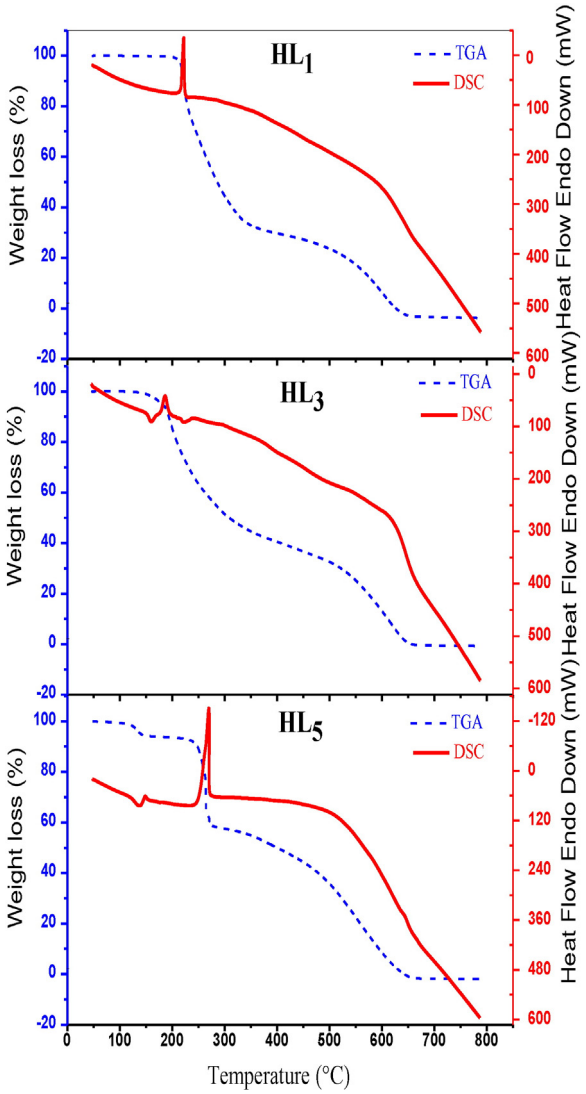

Fig. 12. TGA and DSC thermographs for ligands (HL_1, HL_3 and HL_5).

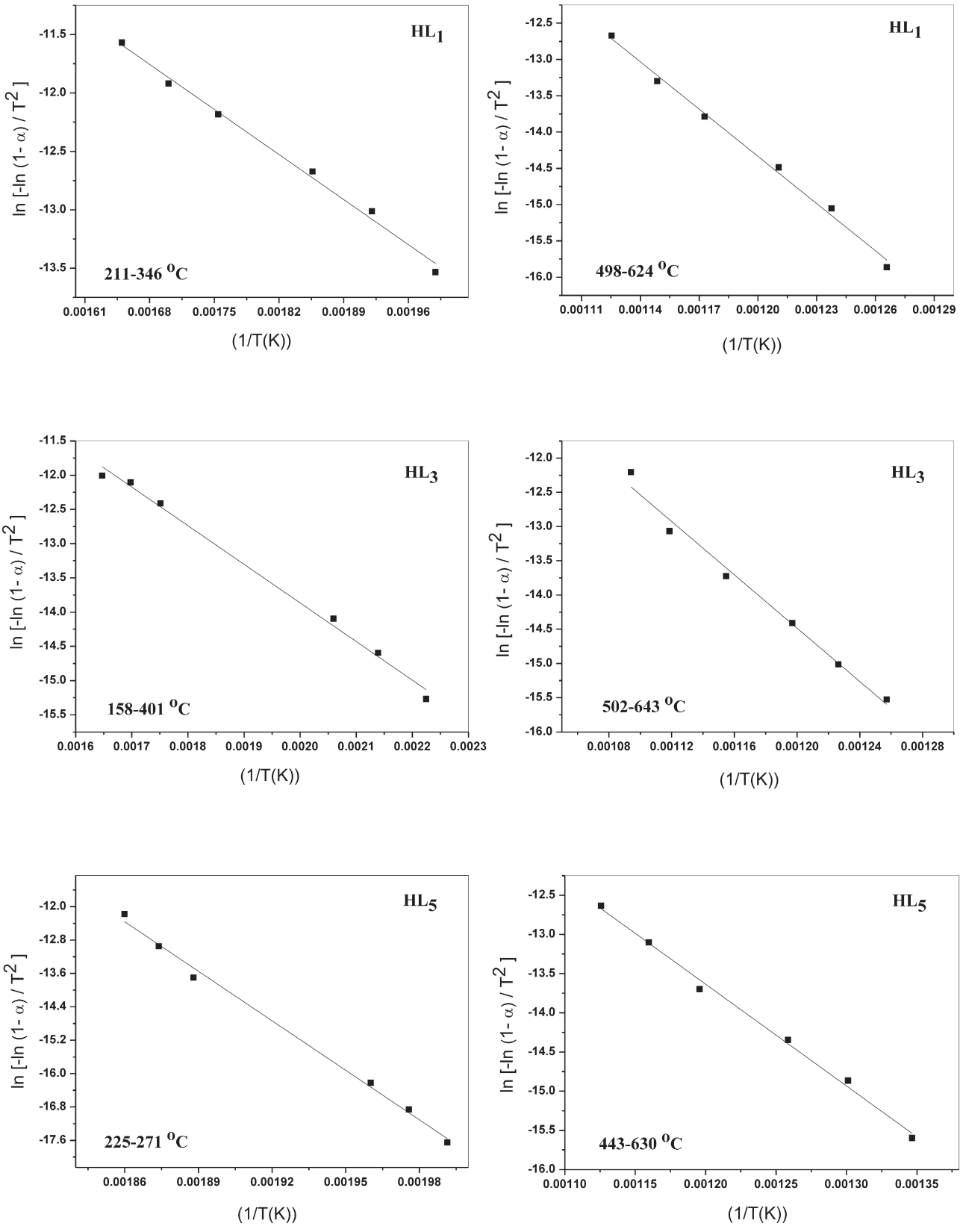

Fig. 13. Coats–Redfern (CR) of the ligands.

4. Conclusions

The present paper reports the synthesis, characterization and their electronic absorption spectra of ligand (azo rhodanine) and M(II)/M(III) complexes. The results of molecular docking between ligands (HL_n) and receptor breast cancer (3HB5) showed a possible arrangement between ligands and receptor (3HB5). The values of ΔN_{max} for HL_n are calculated and found to be in the range of 0.744 - 1.22

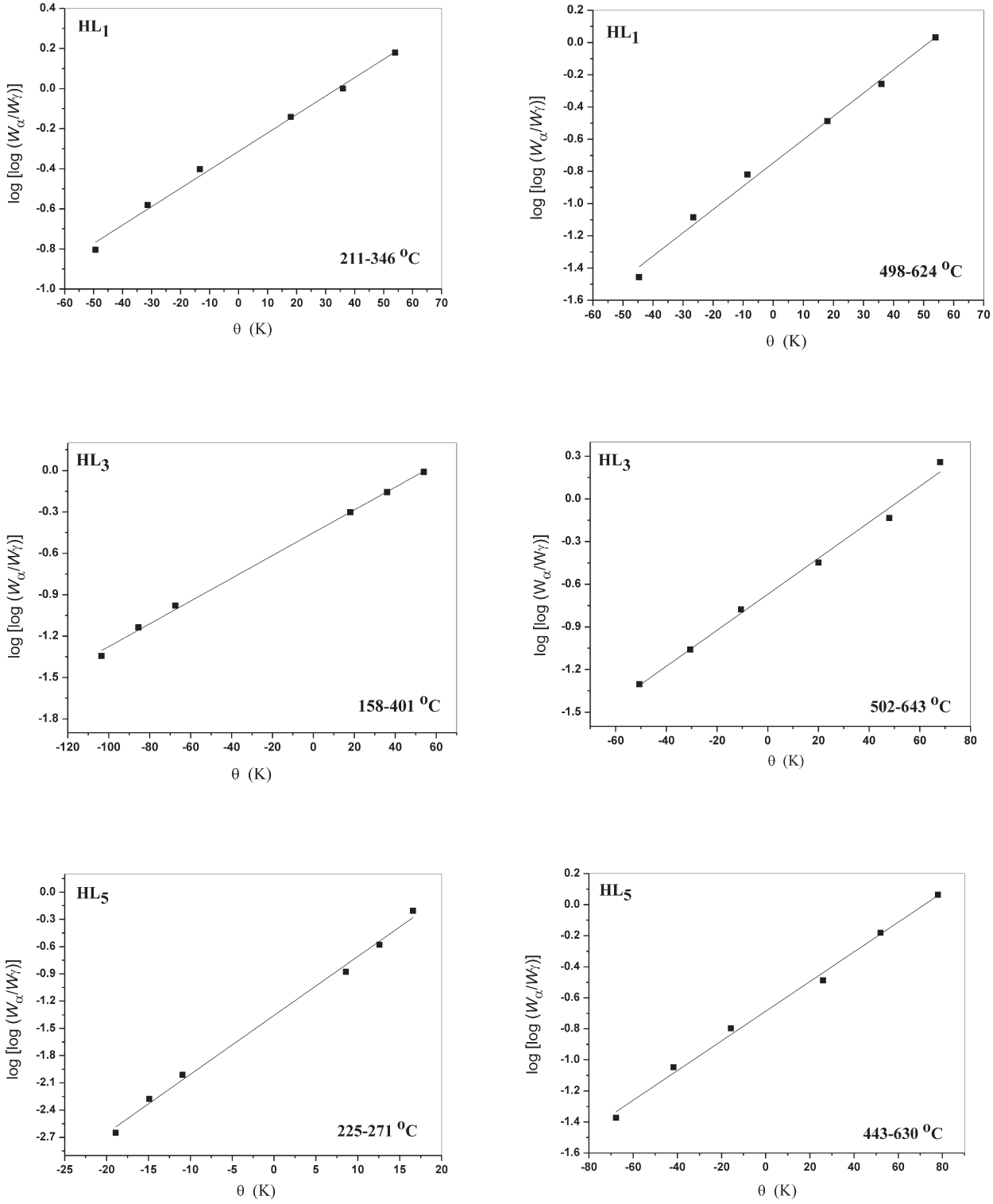

Fig. 14. Horowitz–Metzger (HM) of the ligands.

dependent on the nature of the substituent. It was found that the values of ΔN_{max} for ligands increase with increasing Hammett's constant coefficients (σ^R). The synthetic procedure in this work resulted the formation of complexes in the molar ratio (1:2)(M:L_n), respectively. In these complexes the azo ligand acts as a monobasic bidentate ligand and coordinated to metal ion through the azo-nitrogen, enolic oxygen atoms forming stable six-membered heterocyclic rings. The present study revealed square planar (Pt(II)) and octahedral geometry around M(III)-complexes. From conductance measurements Pt(II)-complexes are non-electrolytes, while M(III) complexes are electrolytic nature. The values of ligand field parameters orbital parameters were calculated. The thermal properties of the ligands and their complexes were investigated by thermogravimetry analysis (TGA) and different thermodynamic parameters are calculated using Coats–Redfern and Horowitz–Metzger methods. The thermogravimetric analysis confirms the presence of coordinated two water molecule in the complexes (**1–6**).

Table 6
Thermodynamic parameters of the ligands.

Compound[a]	Decomposition temperature (°C)	Method	Parameter					r
			E_a (kJ mol^{-1})	A (s^{-1})	ΔS^* (J mol^{-1} K^{-1})	ΔH^* (kJ mol^{-1})	ΔG^* (kJ mol^{-1})	
HL_1	211-346	CR	45.8	7.58×10^1	−214	41.2	159	0.99221
		HM	53.6	4.18×10^2	−200	49	159	0.99398
	498-624	CR	180	4.43×10^8	−87.9	174	247	0.99355
		HM	193	6.40×10^9	−65.8	186	241	0.99169
HL_3	158-401	CR	46.9	7.11×10^1	−215	42.3	161	0.99322
		HM	48.4	1.17×10^2	−210	43.8	160	0.99788
	502-643	CR	162	2.34×10^7	−113	155	250	0.98442
		HM	173	2.50×10^8	−92.2	166	245	0.99156
HL_5	225-271	CR	329	2.54×10^{30}	333	325	151	0.99453
		HM	338	1.70×10^{32}	367	333	142	0.99452
	443-630	CR	108	1.51×10^4	−173	101	242	0.99432
		HM	120	2.05×10^5	−152	113	236	0.99390

References

[1] M.A. Diab, A.Z. El-Sonbati, A.A. El-Bindary, G.G. Mohamed, Sh.M. Morgan, Res. Chem. Intermed. (2015), http://dx.doi.org/10.1007/s11164-015-1946-0.
[2] A.Z. El-Sonbati, M.A. Diab, A.A. El-Bindary, A.M. Eldesoky, Sh.M. Morgan, Spectrochim. Acta A 135 (2015) 774–791.
[3] A.Z. El-Sonbati, M.A. Diab, A.A. El-Bindary, Sh.M. Morgan, Inorg. Chim. Acta 404 (2013) 175–187.
[4] A.Z. El-Sonbati, G.G. Mohamed, A.A. El-Bindary, W.M.I. Hassan, A.K. Elkholy, J. Mol. Liq. 209 (2015) 625–634.
[5] B. Rosenberg, L. Van Camp, J.E. Trosks, V.H. Mansour, Nature (London) 222 (1969) 385–386.
[6] A.M. Eldesoky, M.A. El-Bindary, A.Z. El-Sonbati, Sh.M. Morgan, J. Mater. Environ. Sci. 6 (2015) 2260–2276.
[7] N.A. El-Ghamaz, A.Z. El-Sonbati, M.A. Diab, A.A. El-Bindary, G.G. Mohamed, Sh.M. Morgan, Spectrochim. Acta A 147 (2015) 200–211.
[8] N.A. El-Ghamaz, A.Z. El-Sonbati, Sh.M. Morgan, J. Mol. Struct. 1027 (2012) 92–98.
[9] A.Z. El-Sonbati, M.A. Diab, M.M. El-Halawany, N.E. Salam, Met. Chem. Phys. 123 (2010) 439–449.
[10] N.A. El-Ghamaz, A.Z. El-Sonbati, M.A. Diab, A.A. El-Bindary, M.K. Awad, Sh.M. Morgan, Mater. Sci. Semicond. Process. 19 (2014) 150–162.
[11] M.J. Frisch, G.W. Trucks, H.B. Schlegel, G.E. Scuseria, M.A. Robb, J.R. Cheeseman, J.A. Montgomery Jr., T. Vreven, K.N. Kudin, J.C. Burant, J.M. Millam, S.S. Iyengar, J. Tomasi, V. Barone, B. Mennucci, M. Cossi, G. Scalmani, N. Rega, G.A. Petersson, H. Nakatsuji, M. Hada, M. Ehara, K. Toyota, R. Fukuda, J. Hasegawa, M. Ishida, T. Nakajima, Y. Honda, O. Kitao, H. Nakai, M. Klene, X. Li, J.E. Knox, H.P. Hratchian, J.B. Cross, C. Adamo, J. Jaramillo, R. Gomperts, R.E. Stratmann, O. Yazyev, A.J. Austin, R. Cammi, C. Pomelli, J.W. Ochterski, P.Y. Ayala, K. Morokuma, G.A. Voth, P. Salvador, J.J. Dannenberg, V.G. Zakrzewski, S. Dapprich, A.D. Daniels, M.C. Strain, O. Farkas, D.K. Malick, A.D. Rabuck, K. Raghavachari, J.B. Foresman, J.V. Ortiz, Q. Cui, A.G. Baboul, S. Clifford, J. Cioslowski, B.B. Stefanov, G. Liu, A. Liashenko, P. Piskorz, I. Komaromi, R.L. Martin, D.J. Fox, T. Keith, M.A. Al-Laham, C.Y. Peng, A. Nanayakkara, M. Challacombe, P.M.W. Gill, B. Johnson, W. Chen, M.W. Wong, C. Gonzalez, J.A. Pople, Gaussian 03, Revision C.01, Gaussian, Inc., Wallingford CT, 2004.
[12] T.A. Halgren, J. Comput. Chem. 17 (1998) 490–519.
[13] G.M. Morris, D.S. Goodsell, J. Comput. Chem. 19 (1998) 1639–1662.
[14] M.I. Abou-Dobara, A.Z. El-Sonbati, Sh.M. Morgan, World J. Microbiol. Biotechnol. 29 (2013) 119–126.
[15] A. Beteringhe, C. Racuciu, C. Balan, E. Stoican, L. Patron, Adv. Mater. Res. 787 (2013) 236–240.
[16] A.A. El-Bindary, A.Z. El-Sonbati, M.A. Diab, Sh.M. Morgan, J. Mol. Liq. 201 (2015) 36–42.
[17] N.A. El-Ghamaz, M.A. Diab, A.A. El-Bindary, A.Z. El-Sonbati, H.A. Seyam, Mater. Sci. Semicond. Process. 27 (2014) 521–531.
[18] W.J. Geary, Coord. Chem. Rev. 7 (1971) 81–122.
[19] A.Z. El-Sonbati, M.A. Diab, A.A. El-Bindary, G.G. Mohamed, Sh.M. Morgan, Inorg. Chim. Acta 430 (2015) 96–107.
[20] L.K. Thompson, F.L. Lee, E.J. Gabe, Inorg. Chem. 27 (1988) 39–46.
[21] N.A. El-Ghamaz, A.Z. El-Sonbati, M.A. Diab, A.A. El-Bindary, Sh.M. Morgan, Mater. Res. Bull. 65 (2015) 293–301.
[22] F.C.L.J. Bellamy, The Infrared Spectra of Complex Molecules, Wiley, New York, 1958.
[23] A.Z. El-Sonbati, M.A. Diab, A.A. El-Bindary, Sh.M. Morgan, Spectrochim. Acta A 127 (2014) 310–328.
[24] A.B.P. Lever, Inorganic Electronic Spectroscopy, Elsevier, Amsterdam, 1968.
[25] M.A. Diab, A.Z. El-Sonbati, R.H. Mohamed, Spectrochim. Acta A 77 (2010) 795–801.
[26] J.C. Ballahausen, H.B. Gray, Inorg. Chem. 1 (1962) 111–122.
[27] V.B. Rana, S.K. Sahni, S.K. Sangal, Acta Chem. Scand. 10 (1979) 405.
[28] B.N. Figgis, Introduction to Ligand Field, Wiley Eastern, New Delhi, 1976.
[29] C. Preti, G. Tosi, Transit. Met. Chem. 3 (1978) 17–25.
[30] J. Lewis, B.N. Figgs, Prog. Inorg. Chem. 6 (1964) 105.
[31] N.A. El-Ghamaz, A.A. El-Bindary, A.Z. El-Sonbati, N.M. Beshry, J. Mol. Liq. 211 (2015) 628–639.
[32] A.W. Coats, J.P. Redfern, Nature 20 (1964) 68–79.
[33] H.W. Horowitz, G. Metzger, Anal. Chem. 35 (1963) 1464–1468.